ARTICLES

Ultrafast Vibrational Relaxation and Ligand Photodissociation/Photoassociation Processes of Nickel(II) Porphyrins in the Condensed Phase

Hyo Soon Eom, Sae Chae Jeoung, and Dongho Kim*

Spectroscopy Laboratory, Korea Research Institute of Standards and Science, Taedok Science Town, Yusung, Taejon 305-600, Korea

Jeong-Hyon Ha and Yong-Rok Kim*

Department of Chemistry, Yonsei University, Seoul 120-749, Korea

Received: August 6, 1996; In Final Form: February 11, 1997[⊗]

We have carried out a femtosecond transient absorption spectroscopic study on nickel(II) porphyrins in various solvents in order to obtain detailed information on vibrational relaxation processes occurring in the initial stage after photoexcitation to the highly excited states. We found the decay process of time constant of approximately 1 ps corresponding to the intramolecular vibrational relaxation process for Ni(II)TPP and Ni(II)OEP in toluene. In addition to this process, the intermolecular vibrational relaxation process with 10−20 ps lifetime was also observed for Ni(II)OEP in toluene, although its contribution to the overall decay process is relatively weak probably due to the weak solute/solvent interaction. In coordinating solvents such as pyridine and piperidine, we observed the intramolecular vibrational relaxation processes before complete population of the bottleneck excited metal $^1|0,d_{z^2}\rangle$ or $^3|0,^3(d,d)\rangle$ state. In this case, it is likely that the intermolecular vibrational relaxation process associated with photodissociation/photoassociation processes depending on the selective excitation of four- and six-coordinate species is accompanied by the intramolecular vibrational relaxation due to the strong solute/solvent interaction. These processes are also believed to be responsible for the excess energy dissipation of highly excited nickel(II) porphyrins into the surrounding solvent molecules.

I. Introduction

A great deal of activity has been devoted to a variety of research related to ultrafast photophysical and biophysical processes in the porphyrin molecular systems.[1−3] Some of the ultrafast processes have often been described in terms of a participation of cooling process caused by a short-lived electronic state before the excess energy localized in the molecular system is dissipated.[3] In addition, the photodissociation of axial ligands such as O_2, CO, and NO in heme proteins as well as molecular heating and cooling has long been of considerable interest.[4−9] Metalloporphyrins are ideally suited for study of these processes for the following reasons. First, metalloporphyrins provide a rich diversity of chemical structures and reactions, so that they can serve as model systems mimicking biological functions for the study of a variety of fundamental processes including electronic deactivation, ligand binding/releasing processes, and photooxidation/reduction reactions.[1−3,10−12] Second, transition metal porphyrins have strong electronic transitions in the visible and ultraviolet region, making them experimentally attractive.[13] Third, synthetic and spectroscopic studies of transition metal porphyrins have provided extensive information about the bonding and structure of these molecules.[13] Finally, many studies have been performed on the electronic deactivation kinetics of these molecules on the picosecond and nanosecond time scales which provide a firm basis to identify transient species existing on ultrashort time scales.[1−3,10−12]

The nickel(II) porphyrin is an exemplary system for examining electronic deactivation dynamics and axial ligand photodissociation/association dynamics.[14−19] Of great significance in governing photophysics of the four- and six-coordinate nickel(II) complexes is the presence of a low-lying metal excited (d,d) state having an approximately 250 ps lifetime below the porphyrin ring excited (π,π^*) state. The metal excited (d,d) state shows characteristic derivative-like absorption difference spectra, compared to the featureless diffuse spectra of the ring (π,π^*) and metal ⇔ ring charge transfer excited states.[10,16] This favorable properties of the nickel(II) complexes provide an excellent opportunity for examining deactivation dynamics of photoexcited porphyrin and its interaction with environment that may accompany a transition from an electronic excited state of the macrocycle to an electronic excited state of the metal. During this process nickel(II) complexes then return to their thermal equilibrium via intramolecular vibrational energy redistribution among porphyrin normal modes and intermolecular vibrational redistribution to the surrounding solvent molecular system via solvent/solute interaction.

This study presents the results of transient absorption measurements of four- and six-coordinate nickel(II) porphyrins in noncoordinating and coordinating solvents with femtosecond resolution and unfolds ultrafast processes that may be of general importance in the photophysics of metalloporphyrins.

II. Experimental Section

Nickel(II) porphyrins were purchased from Porphyrin Products (Logan, UT) and used without further purification. The

* To whom all correspondence should be addressed.

[⊗] Abstract published in *Advance ACS Abstracts,* April 15, 1997.

S1089-5639(96)02374-2 CCC: $14.00

ground state absorption spectra of these compounds agree with the previously reported ones.[16] All the solvents used were spectroscopic grade and further purified by fractional distillation.

The dual-beam femtosecond time-resolved transient absorption spectrometer consisted of a self-mode-locked femtosecond Ti:sapphire laser (Spectra Physics, Tsunami), a Ti:sapphire regenerative amplifier (Quantronix) pumped by a Q-switched Nd:YLF laser, a pulse stretcher/compressor, and an optical detection system. A femtosecond Ti:sapphire oscillator pumped by a CW Ar ion laser produces a train of 80 fs mode-locked pulses with an average power of 600 mW at 800 nm. To generate high-energy pulses, the output pulses from the oscillator were stretched and sent to a Ti:sapphire regenerative amplifier pumped by a Q-switched Nd:YLF laser with about 150 ns pulse duration operating at 1 kHz. The femtosecond seed pulses and Nd:YLF laser pulses were synchronized by adjusting an electronic delay between Ti:sapphire oscillator and Nd:YLF laser. Then the amplified pulse train inside the Ti:sapphire regenerative amplifier cavity was cavity dumped by using a Q-switching technique, and about 10 000-fold amplification at 1 kHz was obtained. These pulses were compressed again to reduce the pulse width. The resulting amplified laser pulses had a pulse width of ~150 fs and an average power of 300 mW at 1 kHz repetition rate in the range 790−840 nm. The pump pulses at desired wavelength were generated by frequency doubling in a β-BBO crystal. These pulses were separated by using a dichroic mirror and then focused to a 1 mm diameter spot at the 2 mm path length quartz cell containing the sample. The reflected fundamental beam was focused onto a quartz window to generate a white light continuum, which was again split into two parts. The one part of the white light continuum pulses was overlapped with the pump beam at the sample to probe the transient, while the other part of the beam was passed through the sample without overlapping with the pump beam. The two parts of the white light continuum pulses after the sample were dispersed by a 18 cm focal length spectrograph (Scientific Instruments) and then hit onto the dual 512-channel photodiode arrays (Princeton Instruments). The time delay between pump and probe beams was controlled by making pump beam travel along a variable optical delay line.

To eliminate the signal caused by current leakage (dark current) and variations in the signal strength across the spectrum, accumulations also were taken with no laser shots and with the excitation pulses blocked, allowing only the probe pulses through. The raw intensity data, totaled by the optical multichannel analyzer, is read into a computer after each of the three modes (pump and probe present, no laser pulse present, and probe only present). The entire series of the three modes is then repeated to obtain the satisfactory signal-to-noise ratio. In this way, intensity measurements through excited and unexcited species could then be compared over 150 nm region of the spectrum. Absorption difference measurements for a particular channel were calculated from the formula

$$\Delta A = -\log(I_e(t)/I_r(t))(I_r(0)/I_e(0))$$

where $I_e(t)$ and $I_r(t)$ are the excited and unexcited (relaxed) intensities, corrected for dark current, and $I_r(0)/I_e(0)$ is the ratio between intensities without excitation present. Base line subtraction, signal averaging, and storage were all handled by the computer. The microcomputer also controls other parts of the apparatus, including shutters and optical delay line.

The main idea of the transient absorption spectra is that the continuum probe pulses can be sent before or after the excitation pulses arrives at the sample by changing the optical delay setting. By this sytem, transient absorption spectra are taken as a function of the pump−probe delay to determine the kinetics at multiple wavelengths. Due to the high repetition rate of the laser (1 kHz) and many laser shots average, the signal-to-noise ratio is very large ($\Delta A = \pm 0.005$), depending on the experimental condition.

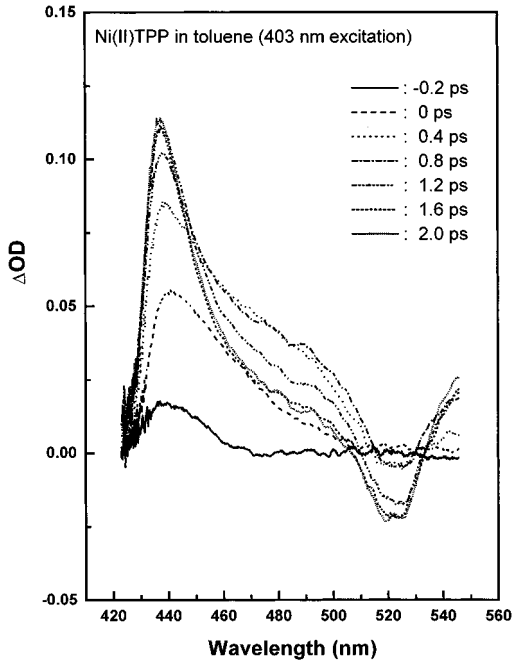

Figure 1. Transient absorption spectra of Ni(II)TPP in toluene after photoexcitation at 403 nm at various time delays between pump and probe pulses. The average intensity of the pump pulses is approximately 8 mW.

For precise measurements of decay profiles of transient absorption signals, the monitoring wavelength was selected by putting an appropriate interference filter (fwhm = 10 nm) and then split into the two parts (probe and reference). With chopping the pump pulses at 40 Hz, the modulated probe pulses as well as the reference ones were detected by a photodiode. The output current was amplified with a homemade fast preamplifier, and then the resultant voltage of the probe pulses was normalized by a boxcar averager with pulse-to-pulse configuration. The resultant signal modulated by a chopper was measured by a lock-in amplifier and then fed into a personal computer for further signal processing.

III. Results

Ni(II)TPP in Toluene. Figure 1 displays the transient absorption spectra of Ni(II)TPP (TPP = tetraphenylporphyrin) in toluene with an excitation of the Soret band at 403 nm at various time delays. The characteristic spectral feature of these absorption spectra shows a featureless broad absorption in the entire probe wavelength region with a dip at 520 nm due to the ground state bleaching for Q band. As a time delay between pump and probe pulses increases, the overall absorption profile narrows to show a transient absorption maximum around 440 nm.

In order to obtain further information, we measured the temporal behavior of transient absorption spectra in both the strong near-UV Soret and the weaker visible Q bands. The transient absorption decay kinetics of Ni(II)TPP in toluene at various wavelengths exhibit biphasic decay profiles (Figure 2). The fitted data of the temporal decay profiles indicate that, as the probe wavelength moves toward blue, the time constants for fast components (τ_1) become larger, and their contributions to the overall decay processes become smaller. The slow

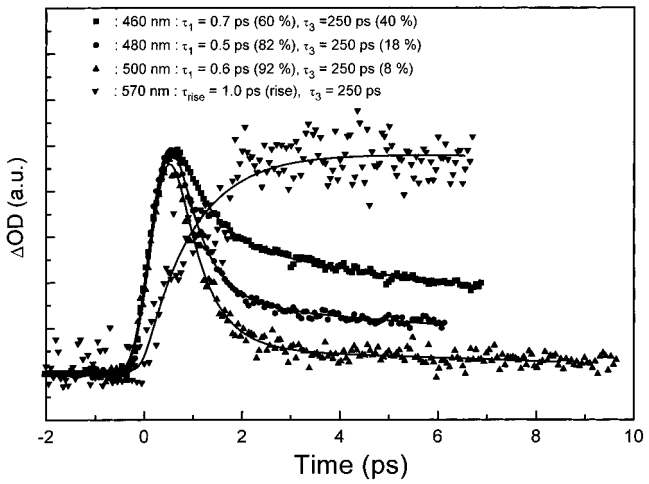

Figure 2. Temporal profiles of transient absorption signals at various probe wavelengths of Ni(II)TPP in toluene after photoexcitation at 407 nm. The τ_3 process represents the electronic decay processes from the metal excited ^{3}(d,d) state to the ground state as reported previously.[14−16] The τ_r process indicates the rise component in the temporal profile of the transient absorption signal. The average power of the pump pulses is about 8 mW.

components (τ_3) with lifetimes of about 250 ps were measured for all the decay profiles and remained the same regardless of the probe wavelengths. This process has been well established to be an electronic deactivation from the metal $^3B_{1g}(d_{z^2},d_{x^2-y^2})$ excited state to the $^1A_{1g}(d_{z^2})^2$ ground state.[14−16] Thus, the time constant of approximately 250 ps for the slow component was fixed in the curve fitting procedure to extract the time constant of the fast decay component in the temporal profiles of the transient absorption signals shown in Figure 2. There is a clear indication of a time lag in reaching the maximum transient absorption value at 570 nm, corresponding to the formation of the relaxed (d,d) state as compared with a fast decay of <1 ps below 500 nm. This largely reflects an ultrafast relaxation processes prior to the formation of the bottleneck excited (d,d) state after photoexcitation to the $S_2(\pi,\pi^*)$ state manifold of Ni(II)TPP in toluene. We have also tried to find out stimulated emission as well as absorption peak in the near-IR region, but no such absorbance change was observed in the entire spectral range (450−850 nm).

Ni(II)TPP in Pyridine and Piperidine. The binding of nitrogenous base ligands such as pyridine and piperidine to the central nickel(II) ions in porphyrin complexes can be described predominantly in terms of the interaction of the ligands with only one metal orbital, namely, the d_{z^2} orbital. The electron content of this orbital can be altered with high quantum efficiency by rapid energy transfer from the photoexcited porphyrin macrocycle to the metal to produce a (d,d) excited state.[16] In this way, it has been possible to interconvert four- and six-coordinate complexes with photons, resulting in observable photodissociation/photoassociation nickel(II) porphyrin adducts.[16] The electronic ground state of the bis-ligated nickel(II) porphyrins is the $^3|0,(d,d)\rangle$[20] state in which the porphyrin ring is in its singlet ground state, while the metal has the paramagnetic ^{3}(d,d) configuration. Complexed species exhibit a Soret band maximum shifted from 416 to 433 nm for Ni(II)TPP. Approximately 60% of the Ni(II)TPP in pyridine is uncomplexed, retaining the diamagnetic $^1A_{1g}(d_{z^2})^2$ ground state.[16]

With the excitation laser pulse at 407 nm, we can photoexcite four-coordinate Ni(II)TPP in a strongly ligating solvent. As the monitoring wavelength moves toward the blue, the time constants for decay profiles become larger. The fitted temporal decay of the transient absorption in pyridine exhibits biphasic

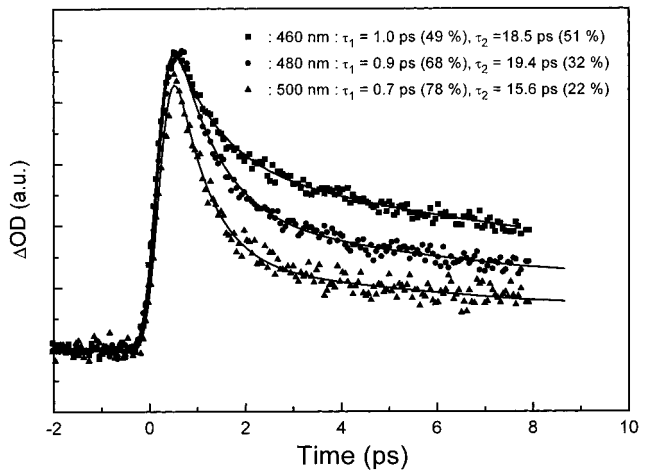

Figure 3. Temporal profiles of transient absorption signals at various probe wavelengths of Ni(II)TPP in pyridine after photoexcitation at 407 nm. The average power of the pump beam is about 8 mW.

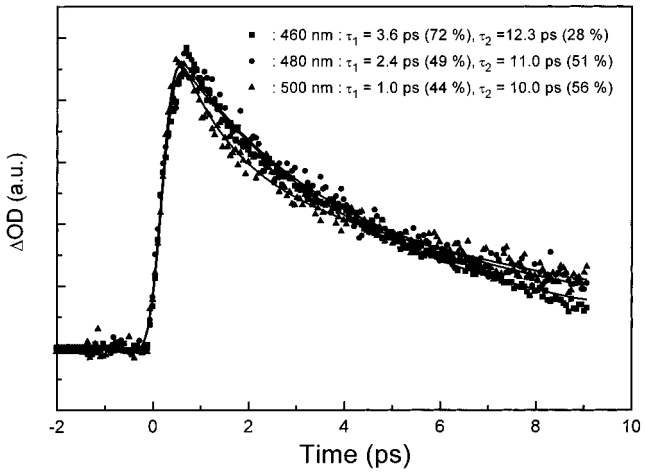

Figure 4. Temporal profiles of transient absorption signals at various probe wavelengths of Ni(II)TPP in piperidine after photoexcitation at 417 nm. The average power of the pump beam is about 8 mW.

decay processes with time constants of less than 1 ps and roughly 10−20 ps (Figure 3). While the fast decay component has a little longer time constant than that observed in toluene, the moderately slow one has not been observed for Ni(II)TPP in toluene. Therefore, the fast decay component is attributable to the same origin of the fast relaxation process (τ_1) in toluene. The latter component (τ_2) can be tentatively explained in terms of an increase in energetic coupling between solute and solvent molecules compared with the similar process in nonligating solvents.

Piperidine is more nucleophilic than pyridine and readily makes six-coordinate complexes with nickel(II) porphyrins. Upon photoexcitation of Ni(II)TPP at 407 nm in piperidine, the residual four-coordinate Ni(II)TPP species are mainly excited, and consequently the decay profiles are similar to those in pyridine (not shown). In order to obtain information on the photodynamics resulting from the axial ligation of piperidine to the central Ni(II) metal, the excitation wavelength was changed to 417 nm, which coincides with the absorption maximum for four-coordinate Ni(II)TPP. However, the transient absorption of Ni(II)TPP in piperidine obtained even by 417 nm excitation is significantly contributed by six-coordinate Ni(II)TPP complexes. The time evolution of the transient absorption for Ni(II)TPP in piperidine (Figure 4) is best described by dual decay times of larger than 1 ps and approximately 10 ps. It should be noted that the time constant of fast component

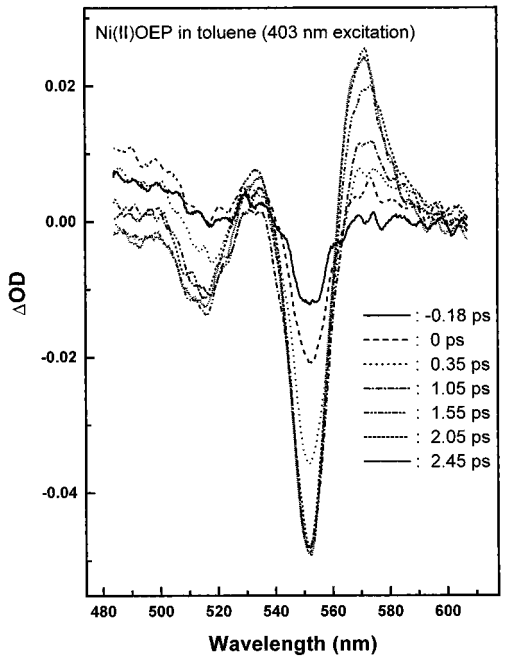

Figure 5. Transient absorption spectra of Ni(II)OEP in toluene after photoexcitation at 403 nm at various time delays between pump and probe pulses. The average intensity of the pump pulses is approximately 8 mW.

becomes larger and that of the slow one becomes smaller than those of Ni(II)TPP in toluene and pyridine. In the meantime, the amplitude of the slow component decreases as the probe wavelength moves toward the blue, which is opposite the case of pyridine solvent. These observations indicate that selective excitation of the bis-ligated Ni(II)TPP exhibits the photodynamics different from that in four-coordinate complexes due to the difference in the initial ground states: the four-coordinate complex has the electronic ground state of $^1|0,d_{z^2}\rangle$ whereas the six-coordinate one does $^3|T^3,(d,d)\rangle$.

Ni(II)OEP in Toluene. The transient absorption spectra of Ni(II)OEP (OEP = octaethylporphyrin) in Figure 5 clearly demonstrate the derivative-like absorption spectra of a typical (d,d) excited state. We observed a time lag of ~1 ps in the growth of transient absorption peak around 570 nm relative to the pulse-limited prompt buildup of the bleaching band at 552 nm (Figure 6). As in the case of Ni(II)TPP in toluene, this behavior indicates that the formation of the relaxed excited (d,d) state has occurred on a ~1 ps time scale through a relaxation process after the photoexcitation to the $S_2(\pi,\pi^*)$ state of Ni(II)OEP.

In order to have further information on the relaxation dynamics, the temporal profiles of transient absorption for Ni(II)OEP in toluene after the excitation at 395 nm were shown in Figure 6. The temporal decay profiles become gradually slower as the probe wavelength moves toward the blue. This feature is consistent with the case of Ni(II)TPP in toluene. In contrast to the case of Ni(II)TPP in toluene, however, the relatively slow component with few tens of picoseconds time constant appears in the temporal profiles of transient absorption changes of Ni(II)OEP in toluene. It is easy to suppose that this alteration of the decay profile should result from the change of the peripheral substituents from TPP to OEP.

Ni(II)OEP in Pyridine and Piperidine. The equilibrium constant for the formation of a six-coordinate complex between Ni(II)OEP and pyridine in the ground state is extremely low compared with that in Ni(II)TPP. The ground state Ni(II)OEP in pyridine remains almost uncomplexed as evidenced by the

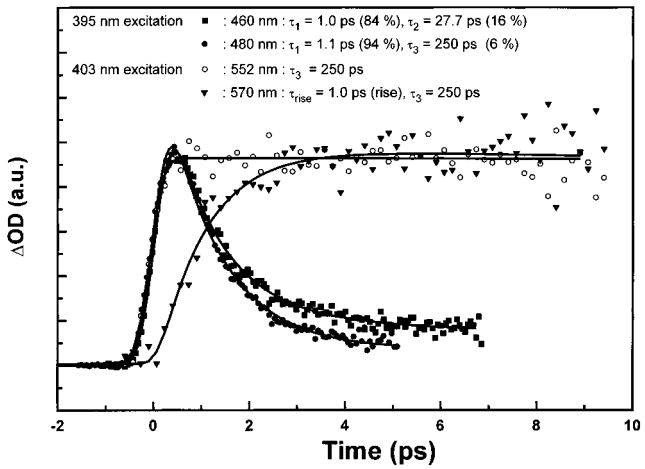

Figure 6. Temporal profiles of transient absorption signals at various probe wavelengths of Ni(II)OEP in toluene after photoexcitation at two different wavelengths. The average power of the pump beam is about 8 mW. The τ_r process indicates the rise component in the temporal profile of the transient absorption signal. The τ_3 process represents the same process as depicted in Figure 2.

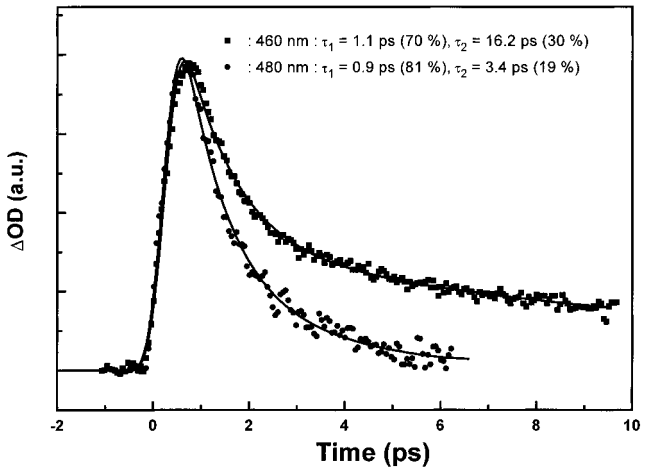

Figure 7. Temporal profiles of transient absorption signals at various probe wavelengths of Ni(II)OEP in pyridine after photoexcitation at 395 nm. The average power of the pump beam is about 8 mW.

essentially identical absorption spectrum with that in toluene.[16a] With an excitation of the Soret band maximum at 395 nm, the transient absorption kinetics shown in Figure 7 exhibits biphasic decay processes with time constants of ~1 and ~10 ps. The temporal decay profiles become gradually slower as the probe wavelength moves toward the blue. This feature is consistent with the case of Ni(II)TPP in pyridine. The smaller contribution of the relatively slow process compared with that of Ni(II)TPP in the same solvent is mainly attributable to the weak solute/solvent interaction of Ni(II)OEP in pyridine as seen in the negligible six-coordinate complex formation in the ground state.[16]

Ni(II)OEP in piperidine readily makes six-coordinate complexes to give a red-shifted Soret band maximum at 420 nm.[16a] We estimate the residual amount of uncomplexed molecule in the ground state to be approximately 25%.[16a] The time evolution of the transient absorption of Ni(II)OEP in piperidine (Figure 8), in which four-coordinate complexes are mainly excited by 395 nm excitation, is best described by a dual-exponential function with time constants of ~1 and ~10 ps, especially in the long wavelength region. In the blue region, the time constant of the fast decay process increases, and then the overall decay profile is dominated by the relatively slow decay processes with lifetimes of ~10 ps. Thus, the overll decay behavior of

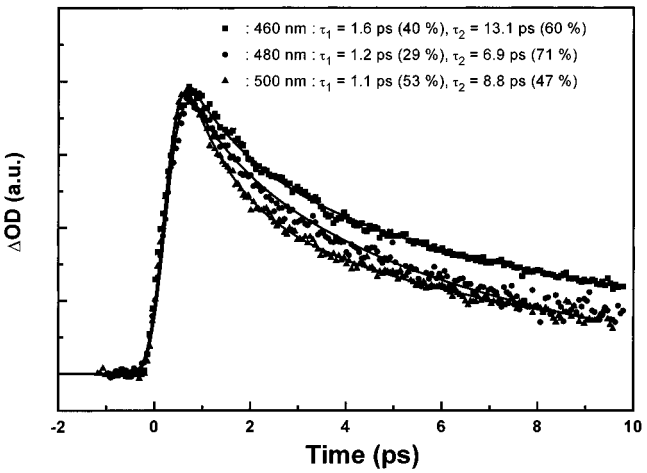

Figure 8. Temporal profiles of transient absorption signals at various probe wavelengths of Ni(II)OEP in piperidine after photoexcitation at 395 nm. The average power of the pump beam is about 8 mW.

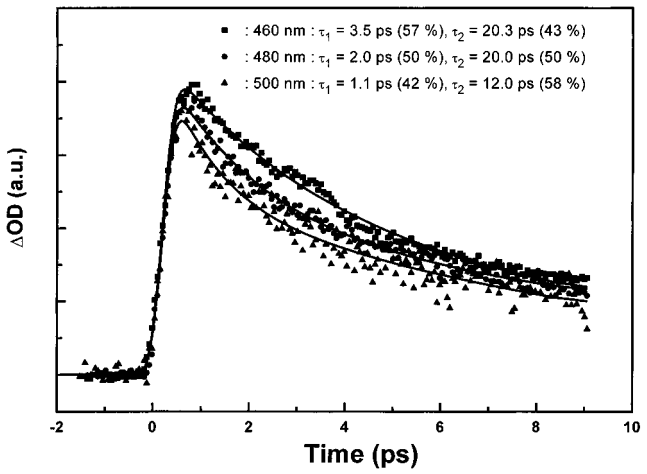

Figure 9. Temporal profiles of transient absorption signals at various probe wavelengths of Ni(II)OEP in piperidine after photoexcitation at 417 nm. The average power of the pump beam is about 8 mW.

photoexcited Ni(II)OEP in piperidine with an excitation of four-coordinate species is quite similar to the case of Ni(II)OEP in pyridine, except that the contribution of the relatively slow component is more significant due to the strong solvent/solute interaction of Ni(II)OEP in piperidine as compared with that in pyridine.

On the other hand, with an excitation of six-coordinate Ni(II)OEP complexes at 417 nm, the transient absorption decay profile is well described by the two decay time constants of larger than 1 and 10−20 ps (Figure 9). The overall feature of the photodynamics of six-coordinate Ni(II)OEP is similar to that for the case of six-coordinate Ni(II)TPP.

IV. Discussion

Before discussing the experimental observations in detail, it is valuable to summarize the rate constants obtained in this work as listed in Table 1. From close examination of the tabulated data, we can extract the following experimental observations for the two nickel(II) porphyrins in this work. First, most of experimental sets, except that for Ni(II)TPP in toluene, exhibit a dual-exponential decay profile with both the fast decay components of lifetimes with 0.5−3.5 ps range and the moderately slow ones with 4−30 ps range. Second, as the probe wavelength moves toward the blue, the decay time constants for both components increase. Third, the evolution of the relaxed (d,d) state of nickel(II) porphyrins in toluene has a time lag of ∼1 ps after photoexcitation to $S_2(\pi,\pi^*)$. Fourth, the change in the peripheral substituent (TPP *vs* OEP) induces an alteration in the decay dynamics. Fifth, the amplitude of the moderately slow component is markedly increased with changing the solvent from the nonligating solvent to the ligating one. Finally, the selective excitation of six-coordinate nickel(II) porphyrins induces an increase in the lifetime for the fast component as compared with that of four-coordinate species.

Characterization of Vibrational Relaxation Processes in (d,d) Excited State of Four-Coordinate Nickel(II) Porphyrins. Upon photoexcitation in the near-UV region, the lowest $S_1(\pi,\pi^*)$ excited state should be formed by rapid deactivation from the initially formed $S_2(\pi,\pi^*)$. However, the fact that stimulated emission was not detected even at the shortest time delay between pump and probe pulses led us to conclude that the lifetime of the lowest porphyrin ring $S_1(\pi,\pi^*)$ state is shorter than our time resolution. The other possible intermediate state, the ring lowest $^3T(\pi,\pi^*)$ state, should manifest its presence with the absorption peak in the near-infrared region (750−850 nm).[10,12] However, such absorptions were not observed in our measurements. These considerations reflect that the absorption of highly vibrationally excited species denotes a very broad spectral feature in the entire visible region at shorter time delays. As these molecular species start to cool and relax to the excited potential well, the absorption of transient species in the red region disappears quickly while the absorption of cooled species, more to the blue, increases. We also do not believe that solvent dynamics makes a dominant contribution to the transient spectral shifts because the position of the Soret band of the four-coordinate species is relatively insensitive to the solvation process.[19]

The above consideration indicates that as the probe wavelength shifts to the blue, the probe pulse monitors the vibrationally cooler species, and consequently a slower temporal decay profile appears. This cooling process can be regarded to be due to two factors. As the internal temperature of the molecular species increases, the molecules locate at the top of the potential well in which the spacing between the energy levels is smaller due to the anharmonicity of the potential. This allows better anharmonic coupling between the vibrational modes of the molecules and the low-frequency internal degrees of freedom (intramolecular vibrational relaxation (IVR)) or the low-energy rotational and translational modes of the solvents which have been shown to be important modes for accepting energy in

TABLE 1: Observed Decay Time Constants (ps) from This Work

			probe wavelength								
			460 nm			480 nm			500 nm		
solute	solvent	excitation wavelength (nm)	τ_1	τ_2	τ_3	τ_1	τ_2	τ_3	τ_1	τ_2	τ_3
Ni(II)TPP	toluene	408	0.7 ± 0.1		250 ± 35	0.5 ± 0.1		250 ± 37	0.6 ± 0.1		250 ± 50
	pyridine	407	1.0 ± 0.2	18.5 ± 3.7		0.9 ± 0.2	19.4 ± 4.0		0.7 ± 0.1	15.6 ± 3.0	
	piperidine	417	3.6 ± 0.7	12.3 ± 2.5		2.4 ± 0.5	11.0 ± 2.0		1.0 ± 0.2	10.0 ± 2.0	
Ni(II)OEP	toluene	403	1.0 ± 0.2	27.7 ± 4.2		1.1 ± 0.2		250 ± 40			
	pyridine	395	1.1 ± 0.2	16.2 ± 2.4		0.9 ± 0.2	3.4 ± 0.6				
	piperidine	395	1.6 ± 0.2	13.1 ± 2.0		1.2 ± 0.2	6.9 ± 1.0		1.1 ± 0.2	8.8 ± 1.3	
		417	3.5 ± 0.5	20.3 ± 3.0		2.0 ± 0.3	20 ± 3.0		1.1 ± 0.2	12.0 ± 1.8	

vibrational relaxation (intermolecular vibrational relaxation (EVR)).[21] As the internal temperature of the molecular species decreases, the difference in temperature between the molecular species and the solvent becomes smaller, and the rate of cooling slows down. The vibrational relaxation process has been studied with time-resolved laser spectroscopic techniques for a number of large dye molecules ($N > 30$ atoms) in a variety of solvents.[22] Some of these studies reported that the rate of IVR for organic molecules in solution depends on the size of molecules where for medium size molecules the IVR process occurs in the 5−8 ps range,[23] but for large size molecules ($N > 30$) the excitation energy is rapidly (≤ 1 ps) redistributed among the vibrational modes of the molecules and then transferred through intermolecular coupling to the solvent on a much slower time scale, roughly 10 ps.[24] The transient Raman measurements[4] and molecular dynamics simulations[6] on heme proteins have provided further evidence that intermolecular vibrational relaxation occurs on a 10−20 ps time scale. Recent UV pump and IR probe investigation showed that it takes 6 ps for photoexcited hemoglobin molecules to completely relax to the cooled species.[25] The universality of this behavior suggests that intermolecular vibrational dynamics is, at least partially, responsible for the decay dynamics occurring on a ∼10 ps time scale. If indeed the redistribution of the excess electronic energy among all the modes of the porphyrin (i.e., intramolecular vibrational relaxation) occurs in less than 2 ps, as has been suggested for other chromophores, then the time constants of less than ∼1 ps we observed for Ni(II)TPP are consistent with the intramolecular vibrational relaxation process. Meanwhile, the components with the time constants of 10−20 ps, which is attributable to EVR processes, were not detected for Ni(II)TPP in this wavelength region. In the case of Ni(II)OEP, however, a 20−30 ps component was observed in addition to the ∼1 ps fast decay processes (Figure 6).

Nickel(II) porphyrins are known to adopt both planar and ruffled conformations in solution, and several Raman lines due to the in-plane skeletal vibrations of the porphyrin macrocycles (ν_2, ν_3, and ν_{10}) are apparently broadened (fwhm = 16−25 cm^{-1}) in the ground state.[26] Courtney et al.[27] observed that these modes become sharper (fwhm = 10−14 cm^{-1}) in the TR^3 (time-resolved resonance Raman) spectra in the τ_3 region, indicating that there should be some conformational relaxation in the τ_2 region of the time scale of 5−10 ps. In this time scale the conformational relaxation such as ruffling modes can contribute to the relatively slow relaxational process which was observed to have 10−20 ps time scales in our transient absorption measurements.[28] Since the IVR process of nickel(II) porphyrins occurs within a ∼1 ps range, the conformational relaxation process is not supposed to contribute significantly to the IVR process. Instead, the conformational relaxation process is believed to be mixed with the EVR process of nickel(II) porphyrins in solution due to the similarity in the time scale of these two processes.

At this moment, it is worthwhile to consider the semiempirical energy gap laws[29,30] which predict an exponential decrease of the relaxation time constant for smaller energy gaps. For instance, the calculation gives a large energy gap between the $S_2(\pi,\pi^*)$ and (d,d) states of 10 000 cm^{-1} for current nickel(II) porphyrins.[31] Although the electronic origin is different, the energy gaps between the $S_2(\pi,\pi^*)$ and $S_1(\pi,\pi^*)$ states of about 5700 cm^{-1} for IR125 dye[32] and 3000 cm^{-1} for oxazine 1 dye[33] were calculated. Experimental time constants of the $S_1(\pi,\pi^*)$ population determined from the onset of stimulated emission are 1.2 ps for IR125 and 200 fs for oxazine 1.[34] The pronounced decrease of the relaxation time for smaller S_2-S_1 gap is in qualitative agreement with the energy gap laws as mentioned above. Although in our case the situation is quite different due to the difference in the electronic configuration between $S_2(\pi,\pi^*)$ and (d,d) states, the difference in energy between these two states is, at least partially, responsible for the time lag of ∼1 ps to build up the excited (d,d) state population (Figures 2 and 6).

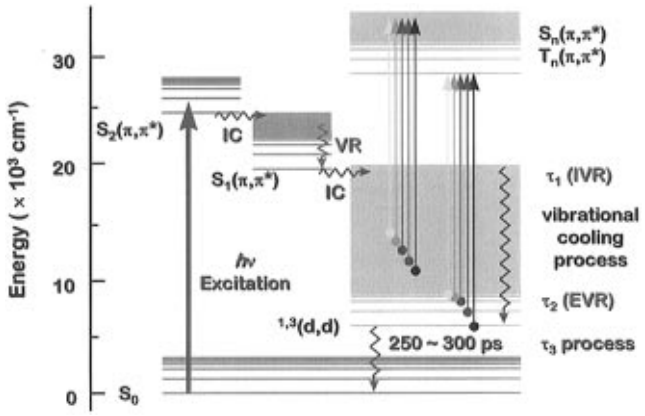

Figure 10. Schematic diagram of the energy relaxation dynamics of nickel(II) porphyrins after photoexcitation to the $S_2(\pi,\pi^*)$ excited state. IC and VR represent the internal conversion and the vibrational relaxation processes, respectively. The energy diagram of each electronic state is based on the calculation of ref 31. The arrows representing the transitions from the (d,d) electronic state manifolds to the upper electronic states on the right-hand side of this diagram denote the probe wavelength energies by the length of each arrow.

In order to give a clear picture related to the photodynamics of nickel(II) porphyrins after the Soret band excitation, a schematic diagram of photodynamic deactivation pathways of nickel(II) porphyrins in nonligating solvent is presented in Figure 10. As shown in the diagram, after the Soret band excitation the fast internal conversion processes to the metal (d,d) excited state through the $S_1(\pi,\pi^*)$ state whose lifetime is expected to be shorter than our laser pulse duration (∼150 fs) due to the lack of stimulated emission from the $S_1(\pi,\pi^*)$ state.[35] Since the energy difference between the $S_1(\pi,\pi^*)$ and ^{3}(d,d) states was estimated to be greater than 10 000 cm^{-1}, the excess energy is large enough to generate vibrationally hot molecular species in the (d,d) electronic state manifold. Due to the anharmonicity of the potential well of the (d,d) electronic state, the vibrational energy spacing is extremely small in the upper part of the excited (d,d) state potential well. Thus, when the molecules start to slide down to the minimum of the potential well, the intramolecular vibrational relaxation presumably dominates the initial stage of cooling processes. As the molecular species become cooler, however, the temperature difference between solute and solvent molecules becomes smaller, and the molecular species start to reach the discrete vibrational levels. At this moment, the solvent fluctuation starts to play an important role in the direct energy transfer between solute and solvent molecules through the fluctuation of solvent motions such as rotational, librational, instantaneous normal modes, etc. Thus, as the molecular species cool, the intermolecular vibrational relaxation through the solute/solvent interaction starts to mainly contribute to the formation of the relaxed excited (d,d) state. In cases such as nickel(II) porphyrins where different modes of the molecules are only weakly coupled, a single internal temperature, calculated as a Boltzmann distribution of the available energy over all the modes of the molecule, is clearly insufficient. Instead, a non-Boltzmann type of distribution of the individual modes is necessary to accurately describe the internal energy distribution in these systems.[36]

Effects on the Vibrational Relaxation Processes of the Different Peripheral Substituents. Keeping in mind the fact that the changes in the Soret band maxima from 416 to 395 nm is accompanied by the change of porphyrin macrocycle from TPP to OEP, the intramolecular vibrational relaxation rate for the two nickel(II) porphyrins was observed to be different from each other: for instance, IVR of Ni(II)TPP at 480 nm and that of Ni(II)OEP at 460 nm in toluene solvent show the lifetimes of 0.5 and 1.0 ps, respectively. In addition, in contrast to the case of Ni(II)TPP in toluene, the relatively slow component with few tens of picoseconds time constant appears in the temporal profiles of the transient absorption changes of Ni(II)OEP in toluene. This feature indicates that the intermolecular vibrational relaxation pathway for Ni(II)OEP to form an excited (d,d) state through vibrational relaxation from highly excited Ni(II)-OEP species is manifest as compared with the case for Ni(II)-TPP. Indeed, even with 35 ps pulse excitation of Ni(II)OEP in toluene in the previous work,[16a] the time lag in the formation of excited metal (d,d) state was clearly observed, which was attributed to the relaxation pathways passing through the ^{1}(d,d) state from the initially excited porphyrin ring (π,π^*) state. From the theoretical consideration on the state energy diagram for nickel(II) porphyrins,[31] two different relaxation pathways to form the ^{3}(d,d) state from the highly excited ring (π,π^*) states of nickel(II) porphyrins can be considered: one through the singlet manifold via ^{1}Q(π,π^*) $\rightarrow$ ^{1}(d,d) $\rightarrow$ ^{3}(d,d) and the other through the triplet manifold via ^{1}Q(π,π^*) $\rightarrow$ ^{3}T(π,π^*) $\rightarrow$ ^{3}(d,d). The structural and peripheral substituents difference between Ni(II)TPP and Ni(II)OEP seems to have an effect on spin−orbit coupling to give rise to a difference in the ratio between the two relaxation routes to form the metal excited ^{3}(d,d) state as well as the contribution of the intermolecular vibrational relaxation.

Very recently, Kruglik et al.[37] found that the pattern of the transient RR (resonance Raman) spectra of Ni(II)OEP in toluene is similar to that of the ground state spectrum, while the frequencies of most Raman bands are appreciably shifted to lower frequencies compared with those of the ground state. From these experimental results, the state responsible for the transient RR spectra was assigned to the metal (d,d) excited state which is generated in subpicoseconds following the excitation to the (π,π^*) state of Ni(II)OEP.[38] These experimental observations also suggest an extremely short lifetime of the S_1(π,π^*) state of nickel(II) porphyrins, which is in accordance with our femtosecond transient absorption results. They also carried out time-resolved anti-Stokes Raman measurements on the totally symmetric ν_4 and ν_7 modes of Ni(II)OEP in toluene.[37] The origin of the appearance of these two anti-Stokes Raman bands is the distribution of excess energy in various degrees of vibrational freedom caused by the large energy difference (ca. 10 000 cm^{-1}) between the initially formed (π,π^*) excited state and the bottleneck metal (d,d) excited state. From the temporal changes of the anti-Stokes Raman bands, they observed that the vibrational cooling processes depend on individual Raman bands (e.g., $\tau_{cooling} = 9$ ps for the ν_4 mode and $\tau_{cooling} = 23$ ps for the ν_7 mode).[37] These observations suggest that the excess energy redistribution process over vibrational degrees of freedom is not uniform. In the meantime, the recent molecular dynamics simulation study on naphthalene molecule[39] revealed that the contribution to the vibrational relaxation process is really dependent upon the mode character. For example, in naphthalene, the A_g modes have weak interactions with other modes so that the energy of the A_{1g} modes does not fluctuate much in vibrational cooling process.[40] It is also considered that the out-of-plane modes are mainly involved in the intramolecular energy transfer process and that the intermolecular energy transfer process works as a major energy transfer channel for optically active in-plane modes. Dipole−dipole interactions of the optically active in-plane modes might enhance the efficiencies of these modes for intermolecular resonant processes.[40] Therefore, the mode-dependent vibrational cooling rates were observed from the time-resolved anti-Stokes Raman measurements of the ν_4 and ν_7 modes of Ni(II)OEP which are probably mainly responsible for the intermolecular vibrational relaxation occurring in the few tens of picoseconds time scales. This behavior is also consistent with our transient absorption experimental results of Ni(II)OEP in toluene. From the considerations for the previous works and the probe wavelength dependence of our transient absorption decay profiles on Ni(II)OEP in toluene, the observed time constants of a few tens of picoseconds might be atributable to both the intermolecular vibrational and the conformational relaxation processes which could not be observed in the transient absorption decay profiles of Ni(II)TPP in toluene.

Effects on Vibrational Relaxation Processes of Axial Ligation of Basic Solvents. On the basis of the ground state absorption spectra between four- and six-coordinate complexes, it is reasonable to suppose that four-coordinate complexes are mainly excited in the case of Ni(II)TPP in pyridine with an excitation at 407 nm and Ni(II)OEP in pyridine and piperidine at 395 nm. Compared with those in nonligating solvents where only four-coordinate complexes are photoexcited, the moderately fast components (10−20 ps) are manifest while the fast components (∼1 ps) exhibit no apparent change for all the above cases.

The rapid decay process was considered to represent the intramolecular vibrational relaxation since the time constants are in accordance with those in toluene. The slow decay process could represent both the electronic population decay and the cooling rate in which the internal temperature of the solute declines as heat is dissipated into the solvent. As the monitoring wavelength moves toward the blue, the time constants for decay profiles become larger, indicating that the intra- and intermolecular vibrational relaxation processes become slower as the cooler species are probed in the blue region. Furthermore, since the dissipation of energy into the solvent occurs during and after the redistribution of energy among the internal modes of the porphyrin, the intermolecular vibrational relaxation is also likely to contribute to the complex decay dynamics that we observed, especially on the slower time scale. As mentioned earlier, the conformational dynamics induced by the existence of both planar and ruffled nickel(II) porphyrins might be involved on a similar time scale. During this process, the photoinduced ligand association process, at least partially, occurs to form six-coordinate complexes as already known in the previous work.[12,16]

The enhancement of intermolecular vibrational relaxation process due to the increase in solute/solvent interaction compared with the same process in nonligating solvents can be explained in terms of the appearance of the decay component with a time constant of 10−20 ps, which was not observed in the nonligating solvent. This proposition was further strengthened from a comparison of the amplitudes of intermolecular vibrational relaxation between Ni(II)TPP and Ni(II)OEP in pyridine. The smaller contribution of this process for Ni(II)-OEP in pyridine is attributable to the weak solute/solvent interaction as seen in the negligible six-coordinate complex formation in the ground state compared with that in Ni(II)TPP in pyridine.[16a]

Characterization of the Vibrational Relaxation Processes of Six-Coordinate Nickel(II) Porphyrins. A change in the pump wavelength from 395 to 417 nm for Ni(II)OEP in

piperidine exhibits an apparent increase in decay time constant while photoexcitation at 395 nm gives the experimental results similar to those in pyridine. Considering the ground state absorption spectra of Ni(II)OEP in piperidine, four- and six-coordinate complexes are selectively excited by 395 and 417 nm pump beams, respectively. The temporal decay profiles for Ni(II)TPP in piperidine upon photoexcitation at 417 nm are also markedly changed in comparison with those for Ni(II)TPP in pyridine with 407 nm excitation. Upon photoexcitation of Ni(II)TPP(pip)$_2$, the previous investigation reported that a prominent excited state absorption feature emerges in the near-IR spectrum which peaks near 840 nm.[12] The $^3|T^3,(d,d)\rangle$ state was suggested to be the most probable candidate for the initially observed excited state, since it has the same multiplicity and the same electronic configuration of metal as the photoinduced excited state $^3|Q,^3(d,d)\rangle$.

This consideration suggests that the fast component observed for Ni(II)TPP in piperidine is probably contributed by the electronic relaxation from the initially formed $^3|T^3,(d,d)\rangle$ state to the excited $^1|0,d_{z^2}\rangle$ state, in which the axial ligand dissociation process occurs due to the increase in the electron density in the d_{z^2} orbital and the vibrational relaxation processes involved in the deactivation pathways. Meanwhile, a recent molecular dynamics simulation of pyridine solvent[41] suggested that the translational and rotational motions are so strongly coupled that adjacent molecules cannot move much without a change of their relative orientation. Thus, once ejected, the basic solvent ligands such as pyridine and piperidine are expected to rotate so that its lone-pair axis will point away from nickel(II) porphyrin *z* axis and effectively lose its interaction with nickel(II) porphyrin molecules on a subpicosecond time scale. Thus, the geminate recombination of ejected axial ligands with the four-coordinate nickel(II) porphyrin does not seem to play a significant role in the photodynamics of these systems. Therefore, it is not unresonable to suppose that the fast component can be related to the intramolecular vibrational relaxation processes as in the cases of toluene and pyridine and the deactivation to the ligand dissociating $^1|0,d_{z^2}\rangle$ state through the initially formed $^3|T^3,(d,d)\rangle$ state.

The relatively slow decay component we observed for nickel(II) porphyrins in piperidine is responsible for both the electronic population decay and the intermolecular vibrational relaxation coupled with the photoinduced ligand dissociation processes. The dominant contribution of these processes to the decay profile of nickel(II) porphyrins in piperidine could be explained in terms of a strong solute/solvent interaction. Especially at the probe wavelength of 500 nm, the time constant of the fast component (τ_1) is approximately 1 ps, indicating that the contribution of IVR process is significant at this probe wavelength (Figures 4 and 8). On the other hand, as the probe wavelength shifts to blue, the τ_1 process of nickel(II) porphyrins in piperidine contributes to the overall decay profiles more significantly in comparison with the cases in toluene and pyridine. We think that the relative ratio in the contribution of the vibrational relaxation dynamics and the electronic deactivation through the initially formed $^3|T^3,(d,d)\rangle$ state is largely dependent on the probe wavelengths. Thus, as the probe wavelength shifts to the blue, the electronic deactivation process becomes more significant than the vibrational relaxation dynamics, resulting in an increase in the amplitude of τ_1 process and its time constant. This behavior is consistent with the previous observation that the characteristic band of triplet state of Ni(II)TPP(pip)$_2$ in the region of 800−900 nm shows double-exponential decay with lifetimes of about 2 and 12 ps, with the amplitude of the short-lived component being twice that of long component.[12] These considerations again support the proposition that τ_1 decay process is to be a mixture of IVR and $^3|T^3,(d,d)\rangle$ state decay processes. Meanwhile, with an excitation at 407 nm of Ni(II)-TPP in piperidine, the residual four-coordinate Ni(II)TPP species are appreciably excited, and consequently the decay profiles are similar to those in pyridine (not shown). This behavior also suggests that the selective excitation of four- or six-coordinate species greatly affects the τ_1 decay processes.

The previous transient absorption measurements also showed that the deactivation from the initially formed $^3|T^3,(d,d)\rangle$ state to the ligand dissociating $^1|0,d_{z^2}\rangle$ state is very fast.[12] The large intersystem crossing rates observed in Ni(II), Ru(II), and Cu(II) porphyrins probably arises from the one-center contribution to the spin−orbit coupling due to the substantial coupling between the ring $e_g(\pi^*)$ and the metal $e_g(d_\pi)$ orbitals.[13] From experimental observations for the photoexcitation dynamics of Ni(II)TPP in noncoordinating and coordinating solvents, we can suggest that when only four-coordinate Ni(II)TPP complexes are pumped like Ni(II)TPP in toluene, the ultrafast intramolecular vibrational relaxation dynamics before the formation of a $^3(d,d)$ excited state is the main process occurring at the initial stage after photoexcitation to the $S_2(\pi,\pi^*)$ state.

On the basis of the results of Ni(II)TPP in piperidine, we can also suggest that the relatively slow decay process for Ni(II)OEP in piperidine is due to the intermolecular vibrational relaxation related to the photoinduced ligand dissociation processes. The fast component observed in the decay profile of Ni(II)OEP in piperidine indicates that there is a intramolecular vibrational relaxation process to give rise to a time lag in the formation of ligand dissociating $^1|0,d_{z^2}\rangle$ excited state from the initially prepared $^3|T,^3(d,d)\rangle$ state by the excitation of six-coordinate Ni(II)OEP complexes (paramagnetic ground $^3(d,d)$ state) at 417 nm. Thus, this indicates that the intersystem crossing from the ring $T(\pi,\pi^*)$ to $S(\pi,\pi^*)$ states is the rate-determining step in the formation of metal excited $^{1,3}(d,d)$ states.

V. Conclusion

The ultrafast intramolecular vibrational relaxation processes with the time constant of approximately 1 ps were observed for both Ni(II)OEP and Ni(II)TPP in toluene. In coordinating solvents such as pyridine and piperidine, depending on selective excitation of four- and six-coordinate species, we also observed that, before complete population of the $^{1,3}(d,d)$ excited state, the intramolecular vibrational relaxation process ($\tau_1 = \sim 1$ ps) is followed by relatively slow energy relaxation process ($\tau_2 =$ 10−20 ps). During this process conformational relaxation might also contribute to the decay processes occurring on the time scale of 10−20 ps, because it is known that nickel(II) porphyrins adopt both planar and ruffled conformers. The time scale of the conformational relaxation was reported to occur in 5−10 ps based on the TR^3 measurements,[27] which is quite compatible with the time scale of the intermolecular relaxation processes investigated in the present work. The comparative investigation on the relaxation process by changing the solvent nature from coordinating to noncoordinating solvent, the excitation wavelength, and peripheral substituents of nickel(II) porphyrins led to a conclusion that the ligand binding/releasing process strongly affects the intermolecular vibrational relaxation process, which is responsible for the excess energy dissipation process of highly excited nickel(II) porphyrins into the surrounding solvent molecules.

Acknowledgment. This work was supported by the grant from the Ministry of Science and Technology and the Center for Molecular Science through the Korea Science and Engineer-

ing Foundation (D.K.) and Good Health R&D Project, 1996 (HMP-96-D-1052), Ministry of Health and Welfare (Y.R.K.), Republic of Korea.

References and Notes

(1) Rodriguez, J.; Kirmaier, C.; Holten, D. *J. Am. Chem. Soc.* **1989**, *111*, 6500.

(2) (a) Dzhagarov, B. M.; Chirvonyi, V. S.; Gurinovich, G. P. In *Laser Picosecond Spectroscopy and Photochemistry of Biomolecules*; Letokhov, V. S., Ed.; Hilger: Bristol, 1987; p 137. (b) Hochstrasser, R. M.; Johnson, C. K. In *Ultrafast Laser Pulses and Applications*; Kaiser, W., Ed.; Springer: New York, 1988; p 357.

(3) Rodriguez, J.; Kirmaier, C.; Holten, D. *J. Chem. Phys.* **1991**, *94*, 6020.

(4) Petrich, J. W.; Martin, J. L.; Houde, D.; Poyart, C.; Orszag, A. *Biochemistry* **1987**, *26*, 7914.

(5) Petrich, J. W.; Poyart, C.; Martin, J. L. *Biochemistry* **1988**, *27*, 4049.

(6) Henry, E. R.; Eaton, W. A.; Hochstrasser, R. M. *Proc. Natl. Acad. Sci. U.S.A.* **1986**, *83*, 8982.

(7) Alden, R. G.; Chavez, M. D.; Ondrias, M. R.; Courtney, S. H.; Friedman, J. M. *J. Am. Chem. Soc.* **1990**, *112*, 3241.

(8) Alden, R. G.; Ondrias, M. R.; Courtney, S. H.; Findsen, E. W.; Friedman, J. M. *J. Phys. Chem.* **1990**, *94*, 85.

(9) (a) Anfinrud, P. A.; Han, C.; Hochstrasser, R. M. *Proc. Natl. Acad. Sci. U.S.A.* **1989**, *86*, 8397. (b) Postlewaite, J. C.; Miers, J. B.; Dlott, D. D. *J. Am. Chem. Soc.* **1989**, *111*, 1248.

(10) Holten, D.; Gouterman, M. In *Optical Properties and Structure of Tetrapyrroles*; Blauer, G., Sund, H., Eds.; de Gruyter: Berlin, 1985; p 64.

(11) Hoshino, M. *Inorg. Chem.* **1986**, *25*, 2476.

(12) Rodriguez, J.; Holten, D. *J. Chem. Phys.* **1990**, *92*, 5944.

(13) Gouterman, M. In *The Porphyrins*; Dolphin, D., Ed.; Academic Press: New York, 1978; Chapter 1.

(14) Kobayashi, T.; Straub, K. D.; Rentzepis, P. M. *Photochem. Photobiol.* **1979**, *29*, 925.

(15) (a) Chirvonyi, V. S.; Dzhagarov, B. M.; Timinskii, Y. V.; Gurinovich, G. P. *Chem. Phys. Lett.* **1980**, *70*, 79. (b) Chirvonyi, V. S.; Dzhagarov, B. M.; Shul'ga, A. M.; Gurinovich, G. P. *Dokl. Akad. Nauk. SSSR* **1981**, *259*, 144.

(16) (a) Kim, D.; Kirmaier, C.; Holten, D. *Chem. Phys.* **1983**, *75*, 305. (b) Kim, D.; Holten, D. *Chem. Phys. Lett.* **1983**, *98*, 584.

(17) Findsen, E. W.; Shelnutt, J. A.; Ondrias, M. R. *J. Phys. Chem.* **1988**, *92*, 307.

(18) Chikisev, A. Y.; Kamalov, V. F.; Korteev, N. I.; Kvach, V. V.; Shkvrinov, A. P.; Toleutaev, B. N. *Chem. Phys. Lett.* **1988**, *144*, 90.

(19) Rodriguez, J.; Holten, D. *J. Chem. Phys.* **1989**, *91*, 3525.

(20) All the state notations come from: Rodriguez, J.; Holten, D. *J. Chem. Phys.* **1990**, *92*, 5944. The ground state, the $^1(\pi,\pi^*)$, and the $^3(\pi,\pi^*)$ configurations of the macrocycle are referred as 0, Q, and T, respectively, and the $(3d_{z^2})^2$ and $(3d_{z^2}, 3d_{x^2-y^2})$ configurations of metal as (d_{z^2}) and (d,d), respectively. The state of the nickel(II) porphyrins is represented as the format $^S|$macrocycle, metal$\rangle$, where *S* is the overall multiplicity of the porphyrins. For instance, the quintuplet state that results from the macrocycle $^3(\pi,\pi^*)$ and the metal $(3d_{z^2}, 3d_{x^2-y^2})$ configurations is denoted as $^5|T,^3(d,d)\rangle$.

(21) (a) Cho, M.; Fleming, G. R.; Saito, S.; Ohmine, I.; Stratt, R. M. *J. Chem. Phys.* **1994**, *100*, 6672. (b) Moore, P.; Tokmakoff, A.; Keyes, T.; Fayer, M. D. *J. Chem. Phys.* **1995**, *103*, 3325. (c) Fleming, G. R.; Cho, M. *Annu. Rev. Phys. Chem.* **1997**, *47*, 109 and references therein.

(22) (a) Wondrazek, F.; Seilmeier, A.; Kaiser, W. *Chem. Phys. Lett.* **1984**, *104*, 121. (b) Seilmeier, A.; Scherer, P. O. J.; Kaiser, W. *Chem. Phys. Lett.* **1984**, *105*, 140. (c) Gottfried, N. H.; Seilmeier, A.; Kaiser, W. *Chem. Phys. Lett.* **1984**, *111*, 326.

(23) (a) Bakker, H. J.; Planken, P. C. M.; Lagendijk, A. *Nature* **1990**, *347*, 745. (b) Green, B. I.; Weisman, R. B.; Hochstrasser, R. M. *Chem. Phys. Lett.* **1979**, *62*, 427. (c) Doany, F. E.; Greene, B. I.; Hochstrasser, R. M. *Chem. Phys. Lett.* **1980**, *75*, 206.

(24) (a) Fujimura, Y.; Lin, S. H.; Schröder, H.; Neusser, H. J.; Schlag, E. W. *Chem. Phys. Lett.* **1979**, *43*, 205. (b) Fujimura, Y.; Nakajima, T.; Lin, S. H.; Schlag, E. W. *Chem. Phys. Lett.* **1979**, *67*, 299.

(25) (a) Lim, M.; Jackson, T. A.; Anfinrud, P. A. *J. Chem. Phys.* **1995**, *102*, 4355. (b) Lim, M.; Jackson, T. A.; Anfinrud, P. A. *Science* **1995**, *269*, 962.

(26) (a) de Paula, J. C.; Walters, V. A.; Nutaris, C.; Lind, J.; Hall, K. *J. Phys. Chem.* **1992**, *96*, 10591. (b) Walters, V. A.; de Paula, J. C.; Babcock, G. T.; Leroi, G. T. *J. Am. Chem. Soc.* **1989**, *111*, 8300. (c) Reed, R. A.; Purrello, R.; Prendergast, K.; Spiro, T. G. *J. Phys. Chem.* **1991**, *95*, 9720.

(27) Courtney, S. H.; Jedju, T. M.; Friedman, J. M.; Alden, R. G.; Ondrias, M. R. *Chem. Phys. Lett.* **1989**, *164*, 39.

(28) (a) Sparks, L. D.; Anderson, K. K.; Medforth, C. J.; Smith, K. M.; Shelnutt, J. A. *Inorg. Chem.* **1994**, *33*, 2297. (b) Jentzen, W.; Simpson, M. C.; Hobbs, J. D.; Song, X.; Ema, T.; Nelson, N. Y.; Medforth, C. J.; Smith, K. M.; Veyrat, M.; Mazzanti, M.; Ramasseul, R.; Marchon, J.-C.; Takeuchi, T.; Goddard III, W. A.; Shelnutt, J. A. *J. Am. Chem. Soc.* **1995**, *117*, 11085. (c) Hobbs, J. D.; Majumder, S. A.; Luo, L.; Sickelsmith, G. A.; Quirke, J. M. E.; Medforth, C. J.; Smith, K. M.; Shelnutt, J. A. *J. Am. Chem. Soc.* **1994**, *116*, 3261.

(29) Englman, R.; Jortner, J. *Mol. Phys.* **1970**, *18*, 145.

(30) Murata, S.; Iwanaga, C.; Toda, T.; Kokobun, H. *Ber. Bunsen-Ges. Phys. Chem.* **1972**, *76*, 1176.

(31) (a) Ake, R. K.; Gouterman, M. *Theor. Chim. Acta* **1970**, *17*, 408. (b) Antipas, A.; Gouterman, M. *J. Am. Chem. Soc.* **1983**, *105*, 4896.

(32) (a) Hasche, T.; Ashworth, S. H.; Riedle, E.; Woerner, M.; Elsaesser, T. *Chem. Phys. Lett.* **1995**, *244*, 164. (b) Ashworth, S. H.; Hasche, T.; Woerner, M.; Riedle, E.; Elsaesser, T. *J. Chem. Phys.* **1996**, *104*, 5761.

(33) Mokhtari, A.; Chebira, A.; Chesnoy, J. *J. Opt. Soc. Am. B* **1990**, *7*, 1551.

(34) Laermer, F.; Elsaesser, T.; Kaiser, W. *Chem. Phys. Lett.* **1989**, *156*, 381.

(35) Ohta, K.; Naitoh, Y.; Saitow, K.; Tominaga, K.; Hirota, N.; Yoshihara, K. *Chem. Phys. Lett.* **1996**, *256*, 629.

(36) Sato, S.; Kitagawa, T. *Appl. Phys. B* **1994**, *59*, 415.

(37) Kruglik, S. G.; Mizutani, Y.; Orlovich, V. A.; Kitagawa, T. In *Proceedings of the XVth International Conference on Raman Spectroscopy*; Asher, S. A., Stein, P. B., Eds.; John Wiley & Sons: New York, 1996; p 122.

(38) Courtney, S. H.; Jedju, T. M.; Friedman, J. M.; Rothberg, L.; Alden, R. G.; Park, M. S.; Ondrias, M. R. *J. Opt. Soc. Am. B* **1990**, *7*, 1610.

(39) (a) Kim, H.; Dlott, D. D.; Won, Y. *J. Chem. Phys.* **1995**, *102*, 5480. (b) Kim, H.; Won, Y. *J. Phys. Chem.* **1996**, *100*, 9495.

(40) Kim, H. Private communication.

(41) Gamba, Z.; Klein, M. L. *Chem. Phys.* **1989**, *130*, 15.